Article

Granger Causality Analysis of Geophysical, Geodetic and Geochemical Observations during Volcanic Unrest: A Case Study in the Campi Flegrei Caldera (Italy)

Simona Tripaldi [1,*], Sergio Scippacercola [2,3], Annarita Mangiacapra [3] and Zaccaria Petrillo [3]

[1] Dipartimento di Scienze della Terra e Geoambientali, Università degli Studi di Bari "Aldo Moro", Campus Universitario, via Orabona 4, 70125 Bari, Italy

[2] Dipartimento di Economia, Management, Istituzioni, Università degli Studi di Napoli "Federico II", via Cinzia, 80128 Naples, Italy; sergio.scippacercola@unina.it

[3] Istituto Nazionale di Geofisica e Vulcanologia, Sezione di Napoli—Osservatorio Vesuviano, 80124 Naples, Italy; annarita.mangiacapra@ingv.it (A.M.); zaccaria.petrillo@ingv.it (Z.P.)

* Correspondence: simona.tripaldi@uniba.it; Tel.: +39-080-544-2580

Abstract: The recent signs of reawakening at Campi Flegrei caldera (Southern Italy) received a great deal of attention due to the issues related to the volcanic risk management in a densely populated area. This paper explores relations between ground deformations, seismicity and geochemical time series in the time span 2004–2016. The aim is to unravel primary processes of unrest and the related indicators which may change in time. Data structure and interactions among variables were examined applying the clustering analysis, the correlations and the Granger causality test. The hierarchical agglomerative clustering detected two sub-periods which were further investigated. In both sub-period causal links were observed between variables while correlations did not appear and vice versa. Thus, well established formal approaches are required to study causal relations. Granger test results indicate that during 2004–2011 the awakening unrest could be mainly ascribed to hydrothermal system pressure fluctuations, probably induced by deep-rooted fluids injection, and that ground deformation together with CO_2/H_2O appears the most suitable geo-indicators. The 2011–2016 sub-period is characterized by enhanced dynamical connectivity. Granger test results suggest that the unrest is driven by a more localized and shallower thermohydromechanical engine. CO/CO_2, He/CH_4 and ground deformation velocity are mutually interacting appearing the most suitable geo-indicators.

Keywords: Granger test; ground deformation; degassing; seismicity; volcanic unrest

1. Introduction

Accurate knowledge of volcanic structures and behavior needs the definition and the understanding of several major processes, an ongoing task that can be undertaken via physical and mathematical parametrization (modeling) or via purely statistical approaches [1,2]. Despite the progressive improvements made by the scientific community, some issues are still unresolved. A major challenge concerns the study of unrest processes aimed to forecast.

It has long been recognized that deformation, seismicity and degassing are the main indicators of volcanic unrest [3]. However, these direct observations are all the expression of endogenous processes on Earth's surface. How driving forces influence external manifestations requires the study of complex temporal interactions meanwhile competitive (e.g., fracturing and sealing processes) and/or synergic (e.g., pressurization in a spatially correlated heat source and tectonically week zones) processes may

occur. This is just the case of magmatic-hydrothermal systems. Temperature/pressure changes within the magmatic reservoir and hydro-mechanical changes within the hydrothermal system can both drive to unrest. Critical factors to this kind of study are the time dependence of the studied variables on the state of the system, which may generate spurious correlations [4,5]. Thus, retrieving the relative contribution of primary processes from the behavior of indirect observations, implicitly requires the study of causality. This task can be faced via statistical approaches, which use predictability to identify causation between time series variables.

Statistical short-term forecasting, dynamic behavior of time series and causality may be assessed performing the vector autoregressive (VAR) model [6], which is a multi-equation system where all the variables are treated as endogenous (dependent). In this work, we address the uncertainty issues related to the understanding of volcanic unrest exploring hypotheses about statistical order applying the Granger causality test [7,8]. A time series variable X is said to "Granger-cause" variable Y if past values of X helps to predict Y, better than just the past values of Y do. The method, originating in econometrics, has enjoyed increasing popularity in many other fields of sciences. Applications to climatic [9–12] environmental/ecological [13–16], hydrogeological [17] and neurobiological [18–21] measures both in time and frequency domain are reported. However, as far as we know, the Granger causality test has never been applied in volcanological contexts.

Data availability for the Campi Flegrei caldera (CFc), a semiplugged felsic caldera located in Southern Italy, provides a great opportunity to investigate the volcanic-hydrothermal forcing with the Granger causality test. The current unrest phase at CFc began in 2005 and it is still ongoing [22–24]. Compared to the past ones, this unrest period is characterized by a progressive uplift, the occurrence of shallow (<4 km) microseismicity and the increase in the flux of the magmatic gases. Both volcanic and non-magmatic hydrothermal unrest are plausible mechanisms responsible for the recent CFc crisis [3,25].

In the current study, we used ground deformations, seismicity and geochemical (CO_2/H_2O, He/CH_4, CO/CO_2) time series variables recorded by the volcanic monitoring networks at CFc in the time span 2004–2016. Our aim is to understand their behavior looking for causal relations to unravel the primary process of unrest and the related indicators.

2. Study Area

The CFc is a volcanic complex located in the Campanian Plain, Southern Italy (Figure 1). During its history, the caldera has experienced notably large explosive events. The eruptions of the Campanian Ignimbrite and the Neapolitan Yellow Tuff [26–28] led to the formation of its primary structure. It consists of a subcircular depression composed of two nested collapses (Figure 1) infilled by Plio-Quaternary continental and marine sediments and by volcanic deposits [29]. The more recent Agnano Monte Spina and Astroni explosive eruptions modified the caldera structure, as did the numerous successive eruptions, thereby generating pyroclastic deposits spread over an extremely large area [30]. The last eruption in CFc occurred in AD 1538 [31], which demonstrates that the caldera magmatic system is still active. The Solfatara-Agnano area (Figure 1) hosts fumaroles, mud pools and hot springs which testify to intense hydrothermal activity. The dynamic of this volcanic structure was strongly sensed by the bradyseismic episodes that occurred in 1969–1972 and 1982–1984, which generated a rapid uplift of 3.5 m around the town of Pozzuoli [32,33]. Notably, the 1982–1984 crisis was accompanied by more than 15,000 shallow earthquakes [34]. Successively, ground subsided until 2005, when a new uplift process began, and it is still ongoing. This new phase of unrest, different from the previous ones, is characterized by a smaller number of shallow earthquakes of low magnitude and an increase of fumaroles emissions rates and temperatures [35] which caused great concern. Despite numerous studies being carried out for the understanding of the CFc structures and related dynamics, several issues are still under debate. Here, we report some key features, derived by geophysical studies, of the deep to shallow structure of the caldera: (i) a low velocity zone interpreted as magmatic source at 7.5 km depth overlined by a limestones basement whose top locates at about 4 km depth [36,37]; (ii) a low Vp/Vs anomaly likely

related to a fractured supercritical gas-bearing formation at about 4 km depth beneath the city of Pozzuoli [38,39]; (iii) a 1 km wide aseismic area of high attenuation located SE of Pozzuoli at 4–4.5 km depth maybe related to an intrusion occurred during the 1984 bradyseismic crisis, and a seismic high attenuation zone at about 3–4 km of depth interpreted as fractured over-pressured gas-bearing formations [40,41]; (iv) a low Vp/Vs and high Qp and Qs seismic layer at 2 km depth underneath the CFc caldera with its central most permeable part (a low Vp/Vs and low Qp and Qs) in correspondence of the Pozzuoli area interpreted as a structure responsible of the magmatic fluids migration from the deep magma reservoir to the shallow Pozzuoli geothermal reservoir [42]; (v) a resistive plume underneath the Solfatara crater down to 2–3 km depth associable to steam/gas within the hydrothermal system [43,44]; (vi) a conductive layer related to a fractured clay cap confined in the first 500 m of depth below the Solfatara–Pisciarelli area [43]; (vii) a resistive unit interpreted as a gas dominated reservoir located 60 m beneath the Bocca Grande fumarole and connected to the vent [45]. Besides, geochemical studies greatly contributed to the knowledge of the CFc volcanic processes and of the ground displacement source, suggesting conceptual models [22,35,46,47] accounting for fumarolic gas chemistry changes, diffuse CO_2 soil degassing and temperature increase, physical simulations and geophysical observations. The recent unrest was interpreted as driven by batches of injected fluids, released at shallow depth (about 4 km) by decompressing magmas at a critical degassing pressure and entering the hydrothermal system [35]. Consistently, background seismicity and soil degassing of CO_2 fluctuations result are controlled by the temperature and pressure increase of the hydrothermal system [23,48]. On the contrary, other authors argue that the ongoing unrest is not related to the activity of a shallow evolving degassing magma, but rather due to magmatic fluids, ascending directly from the deep (8 km) regional magmatic reservoir [47]. Summing up, a debate is still open about the nature of the source, and its relative depth, of the CFc unrest processes. With the present study, we aim to contribute to a better understanding of the processes temporal sequence, using a statistical approach applied to geochemical and geophysical time series. By means of the Granger causality relationship, we look for insights into the most suitable geo-indicators of unrest processes.
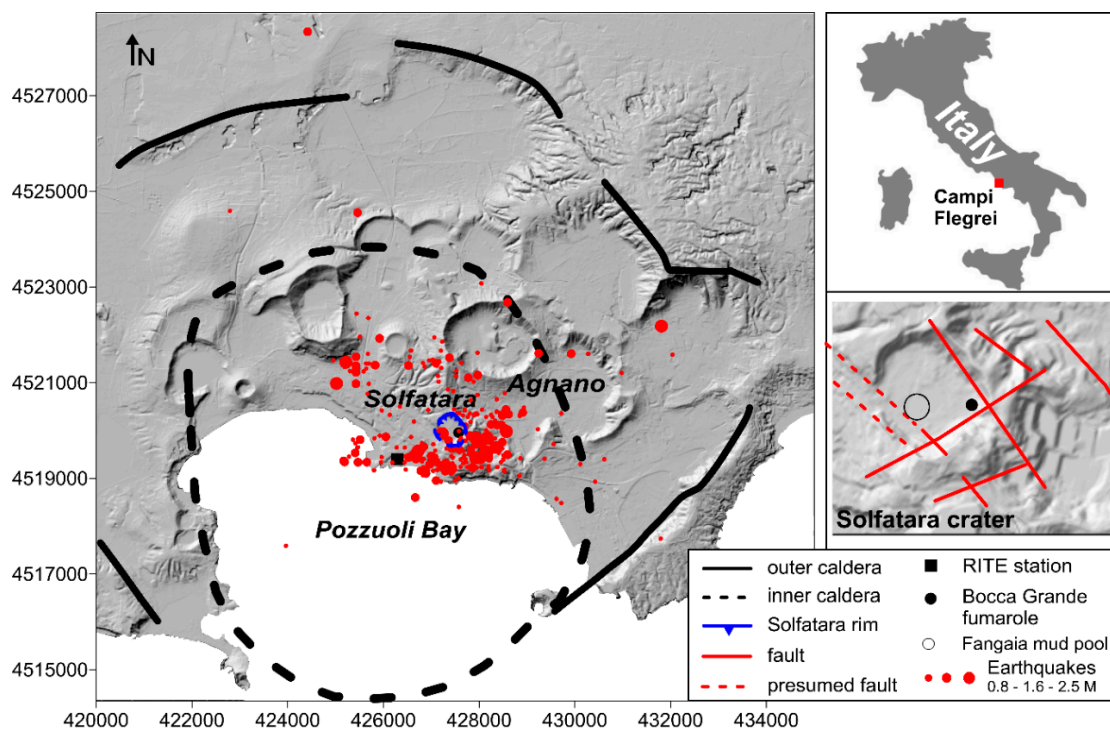
Figure 1. Campi Flegrei caldera map and Solfatara crater. Structures are reported from [29,49].

3. Materials and Methods

3.1. Dataset

The geodetic (GPS) dataset is composed of monthly averaged elevation changes (Figure 2a) from January 2004 to December 2016 recorded at the RITE station [50,51] (Figure 1). Ground deformation data are recorded at a 30 s sampling rate [50] allowing for an accurate estimate of the associated errors. Here, we use monthly data for which the associated mean error is about ± 0.2 cm. Note that in Figure 2a the dots are thicker than 0.5 cm. During the studied period, the minimum value is found in March 2005, and afterwards, an uplift period starts. The uplift period is characterized by a fastening increasing rate and by the superimposition of small-scale episodes of faster uplift (2006 and 2012–2013). Hereafter, this time series will be referred to as GD.

The second dataset consists of volcano-tectonic (VT) monthly number of earthquakes located in the CFc area (Figure 1) and taken from the catalog of Osservatorio Vesuviano, Istituto Nazionale di Geofisica e Vulcanologia [52]. This public catalog reports the space-time events' occurrence with a quality factor based on 3-D ellipsoid location error integrated with the azimuthal coverage of the hypocenter location. The average value of the location error is of the order of some hundred meters. In the period 2004–2016, 570 VT seismic events were located in the Pozzuoli area (Figure 1). The Gutenberg-Richter distribution fit the data with magnitude Md > −0.5. With this cutoff, the number of earthquakes reduces to 507 obtaining the catalog completeness. For the scope of the present work, we are interested in the number of VT events rather than to their magnitude, thus we used the whole dataset composed of 570 events. Preserving the size of the statistical sample should not bias our analysis. Indeed, comparing the data vectors of monthly occurrences obtained with the cutoff at 507 earthquakes (Md > −0.5) with the original one (570 events) we obtained a correlation coefficient of about 0.96. This very high correlation is explicable if the distribution (respect to time) of earthquakes with Md > −0.5 is the same for the earthquakes catalog without cutoff. This time series (hereafter EQ; Figure 2b) appears to have an episodic character and only in the time span 2014–2016 an increasing trend appears. It is worth noting that in the considered time period seismic events are mainly concentrated between the Solfatara crater and the Agnano plain (Figure 1). Moreover, observations are distributed at depths from 0 to 5 km although mainly clustered in the range of 1–2 km (Figure 2c).

Finally, the multivariate dataset includes a monthly averaged time series of fluids compositions discharged at the main fumarolic vent in Solfatara, Bocca Grande ([35,53]; in Figure 1). The geochemical data sampling rate is mainly monthly. The analytical (laboratory data analysis) error is very small with respect to the measured data. Since the geochemical variables are compositional data [54,55], they all were transformed into ratios. Among the available species, CO_2/H_2O, He/CH_4, CO/CO_2 were selected since they are representative of specific volcanic processes. CO_2/H_2O ratio is a useful indicator of magma degassing, He/CH_4 provides information of magmatic fluid contribution in the hydrothermal system and CO/CO_2 is considered the best gas-geothermometer in the hydrothermal system [22,56,57]. He/CH_4 has a quite stable behavior with low variance and a mean value around 0.1 up to 2007 where a first clear peak around June 2007 seems to change the variables dynamic, whereupon a fluctuating trend is observable (Figure 2d). Both CO_2/H_2O and CO/CO_2 (respectively, Figure 2e,f) have an increasing trend in the whole period; these two latter ratios seem to have a more stable behavior showing minor variance.
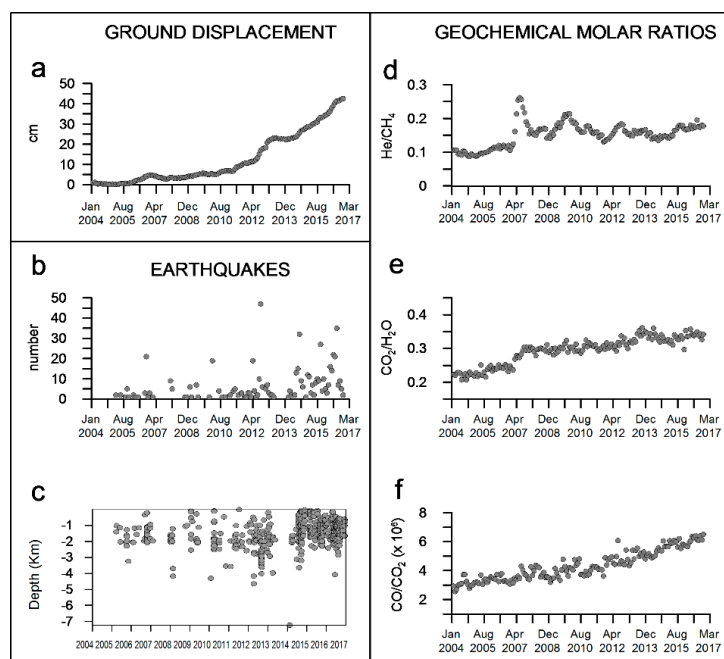
Figure 2. Time variation of (**a**) ground displacement, (**b**) earthquakes number, (**c**) earthquakes hypocentral depths, (**d**) He/CH$_4$ molar ratio, (**e**) CO$_2$/H$_2$O molar ratio, (**f**) CO/CO$_2$ molar ratio.

3.2. Hierarchical Agglomerative Clustering, Correlation and Granger Causality Analysis

The inter-relation structure of the multivariate time series was explored using three statistical approaches: clustering analysis, simple correlations and Granger causality test. These statistical methods analyze different and complementary aspects of the observed data variability to capture data structure and relationships. Moreover, the single time series and their causal relationships are expected to change due to the dynamic nature of the system. Since clustering and correlation analysis have to satisfy the normal distribution, while stationarity is required for Granger analysis, row data were analyzed following the method proposed by [58] to test for normal data distribution. All time series do not validate the Shapiro-Wilk normality test for a confidence level of 95% [59,60]. Thus, row data were logarithmically transformed to reduce variance, skewness and kurtosis [58] and standardized in the whole period to make time series comparable before data mining. A hierarchical agglomerative clustering analysis, based on Ward's method [61,62], was performed to investigate time series similarity among different time periods. Once detected the time grouping based on similarity, Spearman's correlation [63] and Granger causality tests were performed within the detected time groupings.

A vector autoregressive (VAR) model was estimated to perform the Granger causality tests (Appendix A). VAR is an analytic technique used to explain causal relationships among multivariate time series over time, as well as predict future observations. The VAR model [6], fits a multivariate time series regression of each dependent variable on lags of itself and on lags of all other dependent variables. Therefore, each variable is a linear function of past lags of itself and past lags of the other variables. Under appropriate assumptions, the VAR coefficients can be estimated consistently by applying the Ordinary Least Squares (OLS) method to each equation. The distribution of the estimates thus obtained is approximated by a normal distribution.

The effectiveness of a VAR model, and in turn of the Granger test results, depends on the correct postulation of the VAR model and estimation of its parameters [6]. We built the VAR model performing the following steps: data trend test [64,65]; stationarity test of the individual time series within each period with Augmented Dickey-Fuller test [66]; determination of the number of lags based on lag-length selection criteria using AIC (Akaike's information criterion) [67], HQIC (Hannan-Quinn information criterion) [68] and FPE (final prediction error) [69,70]; evaluation of residual autocorrelation by means

of the Lagrange Multiplier (LM) test and assessment of stability with the autoregressive (AR) roots graph [6,71].

Given a VAR model, we may want to know if one variable X "Granger-cause" another variable Y. A method for testing Granger's causality is the regression of Y on the delayed values of Y and X then testing the null hypothesis that the coefficients estimated on the delayed values of X are jointly zero. Failure to reject the null hypothesis is equivalent to failure to reject the hypothesis that X is not Granger's cause Y. The null hypothesis is rejected when the *p*-value is less than 0.05. The Granger's causality does not indicate whether the effect is positive or negative, how long it lasts and whether it derives from another (indirect) variable. Four possible outcomes regarding causal relationships between X and Y exist: (i) absence of any causal relationship (X and Y are independent); (ii) unidirectional causality, X causes Y but Y does not cause X; (iii) unidirectional causality, Y causes X but X does not cause Y; (iv) bidirectional causality between the two variables, X and Y are in feedback.

4. Result

Hereafter are reported the results from the statistical multivariate analysis performed on GD, EQ, CO_2/H_2O, He/CH_4 and CO/CO_2 time series.

The hierarchical agglomerative clustering analysis result is reported in Figure 3a. In the Dendrogram, each leaf (vertex) represents the classified temporal unit and the different heights of the branches (edges) represent the existing ultrametric distance with another branch. The groups differ based on the height of the branches until the next knot of the chart. A suitable choice of the ultrametric distance, at which to make the cut, leads to the identification of groups that have homogeneity within them. According to these criteria, two or three mains groups can be recognized.
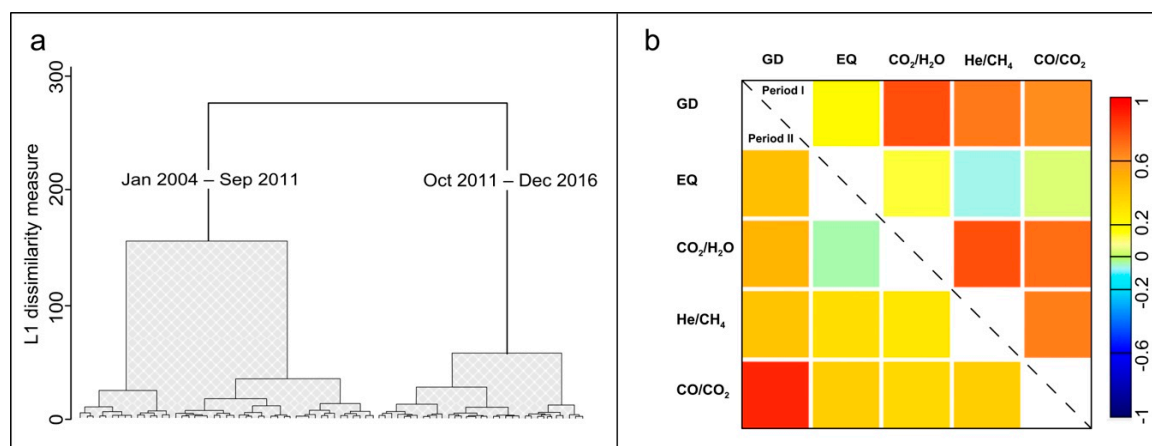
Figure 3. (**a**) Dendrogram of cluster analysis (Ward's method); (**b**) Spearman's correlations among variables in Period I (January 2004–September 2011) and Period II (October 2011–December 2016).

In this regard, it should be reminded that the cluster analysis was performed to detect time windows for which changes on correlations and causal relationships may be revealed. We have chosen to divide the time series into two sub-periods constituted by 93 samples in the time windows January 2004–September 2011 and 63 samples in the time window October 2011–December 2016. This choice seemed the best compromise between reducing potential bias which may derive from the significantly small series length and the resolution loss due to too large series length. Within the two sub-periods, the logarithmically transformed time series results in less dispersion compared to the raw data in the whole period, showing quite a low variance, skewness, and kurtosis (Table A1 in Appendix B).

Correlation analysis results, obtained within the sub-periods January 2004–September 2011 and October 2011–December 2016, are reported in Figure 3b. In the first sub-period, significant, from strong to moderate, correlations exist between: GD and CO_2/H_2O (0.78); CO_2/H_2O and He/CH_4 (0.77); CO_2/H_2O and CO/CO_2 (0.70); GD and He/CH_4 (0.68); He/CH_4 and CO/CO_2 (0.66); GD and CO/CO_2

(0.62). In the second sub-period, fewer correlations appear. Significant correlations are found between GD and CO/CO_2 (0.86) and between GD and CO_2/H_2O (0.50).

In the two sub-periods, all the time series showed trends that were removed. Then, standardization with respect to the mean and the standard deviation within the distinct sub-periods was carried out. Results, based on AIC, HQIC and FPE information criteria, indicate 3–4 lags for the first sub-period (2004–2011) and two lags for the second one (2011–2016). Thus, for the first sub-period, we used three lags, while in the second period residual autocorrelations were detected using two lags. Since the existence of autocorrelation in the residuals may be due to insufficient lags [12,21], three lags were used in the second sub-period, together with the GD first derivative. For this reason, for the second sub-period, we will refer to the velocity of GD (vGD).

Granger test results are reported in Table 1 and we show the unidirectional and bidirectional causality relationships in Figure 4. In the first sub-period GD and CO_2/H_2O, respectively, Granger-cause EQ and He/CH_4. The latter variables are in feedback. EQ Granger-cause CO/CO_2. In the second sub-period, He/CH_4 and CO/CO_2 are in feedback. Weaker feedback appears also between He/CH_4 and vGD as well as between CO/CO_2 and vGD. Moreover, vGD Granger-cause EQ and CO_2/H_2O results to be independent.

Before discussing the obtained results, it is worth noting to remember that Granger causality is not intended as strictly causality but indicates that one thing happens before something else.

Table 1. Granger causality analysis in two different periods with null hypothesis that X does not Granger causes Y ((*) results obtained by differentiating GD).

Granger Causality Wald Test		Jan 2004–Sep 2011	Oct 2011–Dec 2016
Variable Y	**Variable X**	**F (P-value)**	**F (P-value) (*)**
GD	EQ	0.586 (0.6260)	1.212 (0.3167)
GD	He/CH_4	1.394 (0.2525)	2.174 (0.0910)
GD	CO_2/H_2O	0.280 (0.8391)	0.158 (0.9234)
GD	CO/CO_2	1.453 (0.2356)	2.761 (0.0535)
EQ	GD	5.200 (0.0028)	2.721 (0.0561)
EQ	He/CH_4	2.709 (0.0524)	0.399 (0.7544)
EQ	CO_2/H_2O	1.513 (0.2196)	1.179 (0.3290)
EQ	CO/CO_2	1.559 (0.2079)	0.528 (0.6654)
He/CH_4	GD	0.637 (0.5936)	4.219 (0.0065)
He/CH_4	EQ	3.688 (0.0163)	0.269 (0.8473)
He/CH_4	CO_2/H_2O	3.172 (0.0301)	0.579 (0.6317)
He/CH_4	CO/CO_2	1.281 (0.2883)	3.165 (0.0339)
CO_2/H_2O	GD	1.009 (0.3944)	1.810 (0.1596)
CO_2/H_2O	EQ	0.985 (0.4053)	1.456 (0.2398)
CO_2/H_2O	He/CH_4	0.241 (0.8676)	0.679 (0.5696)
CO_2/H_2O	CO/CO_2	0.870 (0.4614)	0.117 (0.9496)
CO/CO_2	GD	0.312 (0.8166)	2.272 (0.0937)
CO/CO_2	EQ	3.543 (0.0194)	0.666 (0.5772)
CO/CO_2	He/CH_4	1.379 (0.2570)	2.634 (0.0619)
CO/CO_2	CO_2/H_2O	1.075 (0.3660)	0.547 (0.6530)
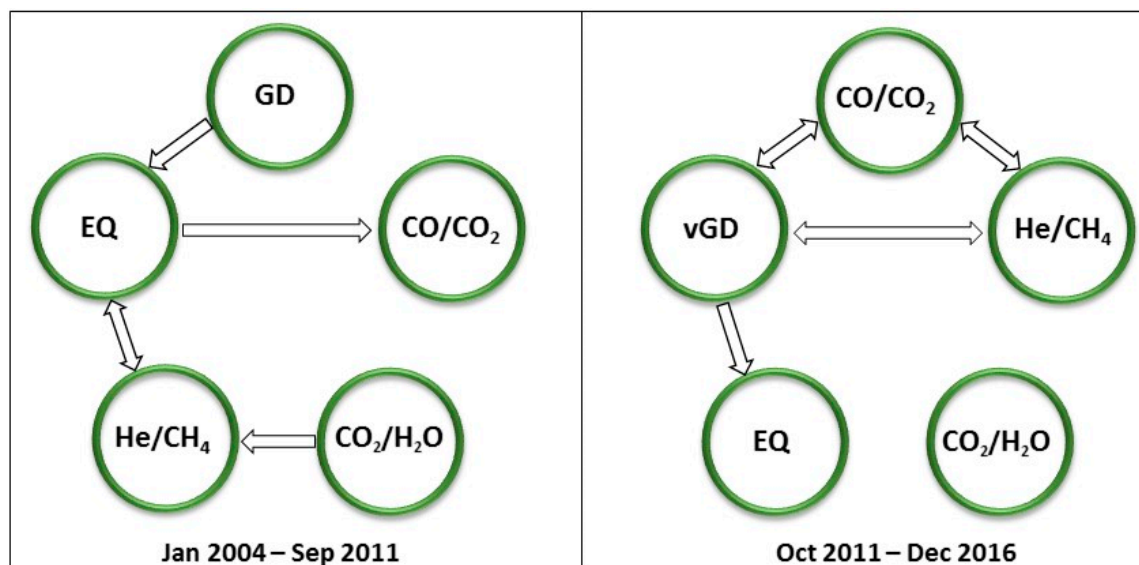
Figure 4. Granger test results for two sub-periods. Arrow indicates Granger unidirectional causality; double-ended arrow indicates Granger bidirectional causality (feedback) between two variables.

5. Discussion

The present work is the first attempt to disclose Granger causal relationships among geo-indicator variables monitored at CFc. Thus, results will be discussed and interpreted at the light of previous studies based on different approaches. The two different explored sub-periods will be firstly discussed separately and finally together.

In the first sub-period, the results of correlation analysis agree with those from the Granger test only as regards the existence of a relation between CO_2/H_2O and He/CH_4, reporting evidence of the interaction between exsolved hot magmatic gases (CO_2-rich) and the hydrothermal system. Since CO_2/H_2O anticipate He/CH_4, we can argue that the injection of deep-rooted CO_2/H_2O at the base of the hydrothermal system drives the increase of magmatic species such as He/CH_4 within the hydrothermal system that feeds the Bocca Grande fumarole. This result is in agreement with observations reported in [22]. The unidirectional causalities found from GD to EQ and from EQ to CO/CO_2 and the bidirectional causality found between EQ and He/CH_4 highlight relations that did not appear from the correlation analysis. In calderas hosting hydrothermal systems, GD and EQ can be associated to magmatic (magmatic bodies/fluids injection or removal) or to non-magmatic processes (groundwater properties fluctuations, poro-elastic transients in the hydrothermal system, regional stress field variations) as well as to their combined action [3,24,72–74]. Both magma intrusion and crystallization can act as a source for pressure–volume changes, and thus provide enough energy for crustal deformation and for rock failure in the brittle domain; rock failure likely provides fractures for fluids transport triggering earthquake swarms. Moreover, short-term oscillations linked to thermohydromechanical disturbances of the hydrothermal system have also been recorded [75]. Fluid migration in both scenarios, magmatic and hydrothermal sources, plays a key role. For CFc, a mechanism involving ground deformation, magmatic fluid migration and earthquakes generated through brittle shear failure processes, has already been proposed by other authors [76,77]. Here, the precedence of GD on EQ, both responding to pressure changes, indicates that deformation fluctuations generate elastic stress acting on rocks which ultimate response is represented by the occurrence of EQ. The precedence of the GD with respect to EQ is probably due to the time necessary for the crustal fluids to ascend through the brittle domain. Since EQ is in feedback with He/CH_4, we can argue that the changes in the volume of magmatic species in the hydrothermal system evolve together with EQ occurrences due to the pore pressure acting on rocks. Indeed, while fluid migration along faults or fractures may promote earthquakes, these last may enhance permeability facilitating

fluid migration [78]. In this framework, EQ anticipates CO/CO_2 which is considered the most sensitive reactive species to temperature [57]. Maybe, CO-rich species reach the surface with a delay which depends on the earthquakes' effectiveness in generating escape routes (cracks and fissures) toward the surface. In this regard, numerical simulations have shown that fumaroles' fluid composition also depends on the rock's properties, like permeability, which controls the timing and the amplitude of their changes through time [79].

In the second sub-period, significant correlations only appear between GD and CO_2/H_2O and between GD and CO/CO_2. Contrastingly, the Granger test, which now accounts for ground displacement velocity (vGD), reveals a denser network of relationships among the variables. Notably, a more complex model with mutually interacting variables points to increased dynamical connectivity. Particularly interesting are the new interactions found for CO/CO_2, which in the first sub-period was only staggered in time by EQ. Here, CO/CO_2 is in feedback with He/CH_4 and with vGD; moreover, He/CH_4 is in feedback with vGD which, in turn, anticipates EQ. As already reported CO/CO_2 is sensitive to temperature variations [57], thus we may derive that temperature fluctuations are evolving together with fluctuations of magmatic species such as He/CH_4 and with deformations. Under hydrothermal conditions, the permeability of fractured rocks depends significantly on the temperature [80]. A laboratory study on representative materials from CFc showed that the Neapolitan Yellow Tuff permeability increases with increasing thermal stressing temperature [81]. Our results indicate a cyclic behavior driven by pressure and thermal stress fluctuations involving sealing and fracturing processes. The pressure and fluid volume increase provoke inflation and temperature growth. Afterwards, the augmented fracturing processes induce pressure dissipation and ground subsidence, by means of the upwards release of fluids. As the pressure dissipates, the fluid flux and temperature both lower with consequent fractures sealing, which in turn determines the pressure increase. The fluid pressure cycling recorded by changes in vGD is finally followed by EQ, as already observed in the first period. Overall, the temperature of the shallow hydrothermal system seems to play a key role along with pressure, thus making thermohydromechanical changes the driving forces. vGD and EQ could represent the mechanical response to the shallow volume–pressure–temperature induced stress. The enhanced connectivity dynamic reasonably reflects an increased velocity of interactions among the variables in this second sub-period.

As just seen, the results of the Granger test are often different from the results of the correlations in terms of relationships found between the variables. The appearance of some relationships in the correlation analysis was not confirmed in terms of Granger causal relationships and vice versa. For example, in the first sub-period, significant correlations exist among GD and geochemical species, especially between GD and CO_2/H_2O and between GD and He/CH_4 but no causal relations are found between GD and CO_2/H_2O and between GD and He/CH_4. This type of discordance may be due to spurious correlations which generate when variables share a common trend or to correlations with an indirect (latent) variable [82]. In complex systems, as the present case, it is not uncommon to come across circumstances in which two variables depend on a third latent variable omitted in the VAR model. For CFc, the relation between ground deformation and fumarolic gas chemistry changes has been linked to different and/or interconnected processes. Hydrothermal and magmatic sources have been proposed [47,83], invoking over-pressured fluids produced by magma crystallization, overpressure of the hydrothermal system due to the emplacement of magma at shallow depths, increase in pore pressures within the hydrothermal system due to active degassing. These different interpretations share a common element which is the pressure changes occurring within the system. In this context, it is immediate to invoke the pressure as a latent variable. However, it cannot be excluded that the failure to reject the null hypothesis may be due to the number of lags or the blanketing effect deriving from the combination of different casual links [82]. Whatsoever, the interesting point here is that during this first sub-period, the only variables that are not preceded by the others are GD and CO_2/H_2O, notably two pressure-driven variables. As for the second sub-period, we note that CO_2/H_2O results

independently. As already stated, this result may depend on the number of the used lags which cannot capture longer-term fluctuations of deep-rooted processes.

Conversely, both in the first and in the second investigated periods, several links not revealed by the correlation analysis were disclosed by the Granger test. This type of discordance is quite common because correlation does not mean causation and unconventional approaches, like Granger test, are generally used to reveal hidden relationships.

This work differs from most existing studies in that it is based on a purely statistical approach to explore the data structure and causal relationships between volcanological variables of interest. Open issues, which could be explored using different geochemical ratios, exogenous data [84] or cross-mapping techniques [13], still remain. However, within the limits (number and type of variables, order model) of the estimated VAR model, the Granger test allowed to reveal the existence of a number of delayed relationships with causalities that are hopefully in certain agreement with studies performed in a similar context [85–87].

6. Conclusions

Ground deformations, seismicity and geochemical time series recorded at CFc were analyzed via a purely statistical approach. Our most striking result derives from the exploration of causal relations made within two distinct sub-periods detected by the cluster analysis. Granger causality results in the first and in second sub-periods are different, reflecting the distinctive features of the volcano driving forces at different unrest stages. Basically, we recognize the contribution of different processes that drive these stages. During 2004–2011, we infer that the unrest awakening could be ascribed by hydrothermal system pressure fluctuations, likely generated by a magmatic process. GD and CO_2/H_2O seem to be the most suitable geo-indicators in revealing the unrest awakening. During the end of 2011 till the end of 2016, the unrest evolution could be ascribed to the thermohydromechanical engine. CO/CO_2, He/CH_4 and vGD seem to be the most suitable geo-indicators of unrest characterized by a higher dynamism. The temporal evolution of the observed seismicity in this period (increase of earthquakes at a depth of < 1 km), suggests a more localized and shallower dynamic. Our results capture interesting features of the recent CFc unrest with a method never applied in volcanic contexts. The proposed analysis is not in competition with the methods traditionally used to study volcanic environments. Conversely, considering that for complex environments any method implies and returns simplifications, we believe that new approaches deserve interest and exploration. Additional information may be further investigated by analyzing other data or using a complementary approach. Identifying causal networks or performing frequency domain analysis could be used to improve our knowledge and forecasting ability in active calderas.

Author Contributions: Conceptualization, S.T. and S.S.; methodology, S.T. and S.S.; formal analysis, S.T. and S.S.; validation, A.M. and Z.P.; resources, Z.P. and A.M.; data curation, Z.P. and A.M.; visualization, A.M.; writing—original draft preparation, S.T.; all the authors contributed to the final version of the manuscript. All authors have read and agreed to the published version of the manuscript.

Conflicts of Interest: The authors declare no conflicts of interest.

Appendix A

A VAR model [7,88] of order p with n variables consists of a system of n equations. In the first equation, the dependent variable is X_1, in the second it is X_2 and so on, until X_n. The regressors of the equations are the values, p delayed, of the other variables of the model. When the number of delays, in all the equations, is equal to p, it is said that the model is of order p and is indicated with VAR (p).

The value of a time series X at a given instant t is calculated as the weighted sum of one's past and past of a set of other variables. Estimating a VAR model means finding the optimal weights in order to minimize estimation errors. For the sake of clarity, we introduce the equations model of order *1*. Indeed, VAR (1) for *n* variables X_i (*I = 1,2, ... , n*) is written as:

$$\begin{cases} X_{1t} = c_1 + \beta_{1,1}X_{1,t-1} + \beta_{1,2}\,X_{2,t-1} + \ldots + \beta_{1,n}\,X_{n,t-1} + \varepsilon_{1,t} \\ \ldots \\ X_{nt} = c_n + \beta_{n,1}X_{1,t-1} + \beta_{n,2}\,X_{2,t-1} + \ldots + \beta_{n,n}\,X_{n,t-1} + \varepsilon_{n,t} \end{cases} \quad (A1)$$

where $\beta_{i,j}$ and c_i are the unknown coefficients, $\varepsilon_{i,j}$ are the error terms (white noise). Equation (A1) is called the unrestricted model because it specifies the full set of available information about all the time series [6]. Equation (A1) can be readily extended to the model of order *p > 1*. Estimation of the parameters of the VAR requires that all the variables in (1) are covariance stationary.

The Granger causality analysis (GCA) is based on the estimation and comparison of two VAR models. Model (1) contains the dependent variable with all the variables of which you want to know the Granger causality. A second VAR model, called restricted model (2), containing only the dependent variables with their delay, is, therefore, estimated. Restricted VAR, that is, omits all variables that are potentially Granger-cause of dependent variables. This leads to a second set of forecasting errors for each variable. Indeed, Equation (A2), referred to as a restricted model, uses only past information of the same variable X_i, and it also can be regarded as the "control" model:

$$\begin{cases} X_{1t} = c'_1 + \beta'_{1,1}X_{1,t-1} + \varepsilon'_{1,t} \\ \ldots \\ X_{nt} = c'_n + \beta'_{n,1}X_{n,t-1} + \epsilon'_{n,t} \end{cases} \quad (A2)$$

where $\beta'_{i,j}$ and c'_i are the unknown coefficients, $\epsilon'_{i,j}$ are the error terms (white noise). If the prediction error for the unrestricted model is significantly lower than the restricted model or if the coefficients relating to the independent variables are significant, then we can say that a variable X_j Granger-cause X_i. In a linear regression model (Equation (A1)) of X_i and X_j, the X_j Granger variable is said to Granger-cause X_i if the inclusion of previous observations of X_j reduces the prediction error (residuals) of X_i, compared to Model (2) that includes only previous observations of X_i. The cause and response *feedback* is established when X_i can Granger-cause X_j and X_j can Granger-cause X_i. Then, the Granger causality from each variable X_i to X_j variable is determined by comparing the estimation accuracies for X_i and X_j of the unrestricted and the restricted models.

Appendix B

Table A1. Statistics of time series in the whole period and in the two sub-periods.

Time Series	Mean	Median	st.dev.	Variance	Skewness	Kurtosis
GD (Jan 2004–Dec 2016)	12.40	5.72	12.33	152.09	0.93	2.56
ln GD (Jan 2004–Sep 2011)	2.71	2.72	0.16	0.02	−0.00	2.14
ln GD (Oct 2011–Dec 2016)	3.58	3.55	0.26	0.06	−0.34	2.34
EQ (Jan 2004–Dec 2016)	3.65	1.00	7.05	49.77	3.23	15.55
ln EQ (Jan 2004–Dec 2016)	0.43	0.00	0.72	0.52	1.75	5.6
ln EQ (Oct 2011–Dec 2016)	1.55	1.61	1.08	1.17	0.10	2.08
He/CH$_4$ (Jan 2004–Dec 2016)	0.15	0.16	0.04	0.00	0.47	4.27
ln He/CH$_4$ (Jan 2004–Sep 2011)	−1.95	−1.88	0.30	0.09	0.09	2.12
ln He/CH$_4$ (Oct 2011–Dec 2016)	−1.84	−1.84	0.09	0.01	−0.12	2.03
CO/CO$_2$ (Jan 2004–Dec 2016)	4.34×10^{-6}	4.18×10^{-6}	1.02×10^{-6}	1.03×10^{-12}	0.45	2.06
ln CO/CO$_2$ (Jan 2004–Sep 2011)	−12.53	−12.53	0.13	0.02	−0.04	2.61
ln CO/CO$_2$ (Oct 2011–Dec 2016)	−12.14	−12.13	0.12	0.01	−0.49	2.89
CO$_2$/H$_2$O (Jan 2004–Dec 2016)	0.29	0.30	0.04	0.00	−0.58	2.26
ln CO$_2$/H$_2$O (Jan 2004–Sep 2011)	−1.31	−1.25	0.13	0.02	−0.41	1.61
ln CO$_2$/H$_2$O (Oct 2011–Dec 2016)	−1.11	−1.12	0.05	0.00	−0.25	2.40

References

1. Cashman, K.V.; Sparks, R.S.J. How volcanoes work: A 25 year perspective. *GSA Bul.* **2013**, *125*, 664–690. [CrossRef]
2. Acocella, V. Great challenges in volcanology: How does the volcano factory work? *Front. Earth Sci.* **2014**, *2*, 4. [CrossRef]
3. Acocella, V.; Di Lorenzo, R.; Newhall, C.; Scandone, R. An overview of recent (1988 to 2014) caldera unrest: Knowledge and perspectives. *Rev. Geophys.* **2015**, *53*, 896–955. [CrossRef]
4. Pearson, K. Mathematical contributions to the theory of evolution, on a form of spurious correlation which may arise when indices are used in the measurement of organs. *Proc. R. Soc. Lond.* **1897**, *60*, 489–498.
5. Box, G. *Time Series Analysis: Forecasting and Control*; Prentice Hall: Englewood Cliffs, NJ, USA, 1994.
6. Lütkepohl, H. *New Introduction to Multiple Time Series Analysis*; Springer: New York, NY, USA, 2005.
7. Granger, C.W.J. Investigating causal relations by econometric models and cross-spectral methods. *Econometrica* **1969**, *37*, 424–438. [CrossRef]
8. Granger, C.W. Testing for causality: A personal viewpoint. *J. Econ. Dyn. Control* **1980**, *2*, 329–352. [CrossRef]
9. Kaufmann, R.K.; Stern, D.I. Evidence for human influence on climate from hemispheric temperature relations. *Nature* **1997**, *388*, 39–44. [CrossRef]
10. Kang, J.; Larsson, R. What is the link between temperature and carbon dioxide levels? A Granger causality analysis based on ice core data. *Theor. Appl. Climatol.* **2014**, *116*, 537–548. [CrossRef]
11. Triacca, U.; Attanasio, A.; Pasini, A. Anthropogenic global warming hypothesis: Testing its robustness by Granger causality analysis. *Environmetrics* **2013**, *24*, 260–268. [CrossRef]
12. Leggett, L.M.W.; Ball, D.A. Granger causality from changes in level of atmospheric CO_2 to global surface temperature and the El Niño–Southern Oscillation, and a candidate mechanism in global photosynthesis. *Atmos. Chem. Phys.* **2015**, *15*, 11571–11592. [CrossRef]
13. Sugihara, G.; May, R.; Ye, H.; Hsieh, C.; Deyle, E.; Fogarty, M.; Munch, S. Detecting Causality in Complex Ecosystems. *Science* **2012**, *338*, 496–500. [CrossRef]
14. Hatala, J.A.; Detto, M.; Baldocchi, D.D. Gross ecosystem photosynthesis causes a diurnal pattern in methane emission from rice. *Geophys. Res. Lett.* **2012**, *39*, L06409. [CrossRef]
15. Detto, M.; Bohrer, G.; Nietz, J.G.; Maurer, K.D.; Vogel, C.S.; Gough, C.M.; Curtis, P.S. Multivariate conditional Granger causality analysis for lagged response of soil respiration in a temperate forest. *Entropy* **2013**, *15*, 4266–4284. [CrossRef]
16. Damos, P. Using multivariate cross correlations, Granger causality and graphical models to quantify spatiotemporal synchronization and causality between pest populations. *BMC Ecol.* **2016**, *16*, 33. [CrossRef] [PubMed]
17. Singh, N.K.; Borrok, D.M. A Granger causality analysis of groundwater patterns over a half-century. *Sci. Rep.* **2019**, *9*, 1–8. [CrossRef]
18. Kamiński, M.; Ding, M.; Truccolo, W.A.; Bressler, S.L. Evaluating causal relations in neural systems: Granger causality, directed transfer function and statistical assessment of significance. *Biol. Cybern.* **2001**, *85*, 145–157. [CrossRef]
19. Ding, M.; Chen, Y.; Bressler, S.L. Granger causality: Basic theory and application to neuroscience. In *Handbook of Time Series Analysis: Recent Theoretical Developments and Applications*; Schelter, B., Winterhalder, M., Timmer, J., Eds.; Wiley-VCH Verlag: Weinhein, Germany, 2006; p. 437.
20. Seth, A.K.; Edelman, G.M. Distinguishing Causal Interactions in Neural Populations. *Neural Comput.* **2007**, *19*, 910–933. [CrossRef]
21. Bose, E.; Hravnak, M.; Sereika, S. Vector Autoregressive (VAR) Models and Granger Causality in Time Series Analysis in Nursing Research: Dynamic Changes Among Vital Signs Prior to Cardiorespiratory Instability Events as an Example. *Nurs. Res.* **2017**, *66*, 12–19. [CrossRef]
22. Chiodini, G.; Vandemeulebrouck, J.; Caliro, S.; D'Auria, L.; De Martino, P.; Mangiacapra, A.; Petrillo, Z. Evidence of thermal-driven processes triggering the 2005–2014 unrest at Campi Flegrei caldera. *Earth Planet Sci. Lett.* **2015**, *414*, 58–67. [CrossRef]

23.   Cardellini, C.; Chiodini, G.; Frondini, F.; Avino, R.; Bagnato, E.; Caliro, S.; Lelli, M.; Rosiello, A. Monitoring diffuse volcanic degassing during volcanic unrests: The case of Campi Flegrei (Italy). *Sci. Rep.* **2017**, *7*, 1–15. [CrossRef]

24.   Petrosino, S.; Cusano, P.; Madonia, P. Tidal and hydrological periodicities of seismicity reveal new risk scenarios at Campi Flegrei caldera. *Sci. Rep.* **2018**, *8*, 1–12. [CrossRef] [PubMed]

25.   Rouwet, D.; Sandri, L.; Marzocchi, W.; Gottsmann, J.; Selva, J.; Tonini, R.; Papale, P. Recognizing and tracking volcanic hazards related to non-magmatic unrest: A review. *J. Appl. Volcanol.* **2014**, *3*, 1–17. [CrossRef]

26.   Rosi, M.; Sbrana, A. Phlegrean fields. *Quaderni Ricerca Scientifica* **1987**, *9*, 114.

27.   Orsi, G.; De Vita, S.; Di Vito, M. The restless, resurgent Campi Flegrei nested caldera (Italy): Constraints on its evolution and configuration. *J. Volcanol. Geotherm. Res.* **1996**, *74*, 179–214. [CrossRef]

28.   Civetta, L.; Orsi, G.; Pappalardo, L.; Fisher, R.V.; Heiken, G.; Ort, M. Geochemical zoning, mingling, eruptive dynamics and depositional processes—The Campanian Ignimbrite, Campi Flegrei caldera, Italy. *J. Volcanol. Geotherm. Res.* **1997**, *75*, 183–219. [CrossRef]

29.   Acocella, V. Evaluating fracture patterns within a resurgent caldera: Campi Flegrei, Italy. *Bull. Volcanol.* **2010**, *72*, 623–638. [CrossRef]

30.   Isaia, R.; D'Antonio, M.; Dell'Erba, F.; Di Vito, M.; Orsi, G. The Astroni volcano: The only example of closely spaced eruptions in the same vent area during the recent history of the Campi Flegrei caldera (Italy). *J. Volcanol. Geotherm. Res.* **2004**, *133*, 171–192. [CrossRef]

31.   Di Vito, M.; Lirer, L.; Mastrolorenzo, G.; Rolandi, G. The 1538 Monte Nuovo eruption (Campi Flegrei, Italy). *Bull. Volcanol.* **1987**, *49*, 608–615. [CrossRef]

32.   Orsi, G.; Civetta, L.; Del Gaudio, C.; De Vita, S.; Di Vito, M.A.; Isaia, R.; Petrazzuoli, S.M.; Ricciardi, G.P.; Ricco, C. Short-term ground deformations and seismicity in the resurgent Campi Flegrei caldera (Italy): An example of active block-resurgence in a densely populated area. *J. Volcanol. Geotherm. Res.* **1999**, *91*, 415–451. [CrossRef]

33.   Del Gaudio, C.; Aquino, I.; Ricciardi, G.P.; Ricco, C.; Scandone, R. Unrest episodes at Campi Flegrei: A reconstruction of vertical ground movements during 1905–2009. *J. Volcanol. Geotherm. Res.* **2010**, *195*, 48–56. [CrossRef]

34.   De Natale, G.; Pingue, F.; Allard, P.; Zollo, A. Geophysical and geochemical modelling of the 1982–1984 unrest phenomena at Campi Flegrei caldera (southern Italy). *J. Volcanol. Geotherm. Res.* **1991**, *48*, 199–222. [CrossRef]

35.   Chiodini, G.; Paonita, A.; Aiuppa, A.; Costa, A.; Caliro, S.; De Martino, P.; Acocella, V.; Vandemeulebrouck, J. Magmas near the critical degassing pressure drive volcanic unrest towards a critical state. *Nat. Commun.* **2016**, *7*, 1–9. [CrossRef] [PubMed]

36.   Judenherc, S.; Zollo, A. The Bay of Naples (southern Italy): Constraints on the volcanic structures inferred from a dense seismic survey. *J. Geophys. Res.* **2004**, *109*, B10312. [CrossRef]

37.   Zollo, A.; Maercklin, N.; Vassallo, M.; Dello Iacono, D.; Virieux, J.; Gasparini, P. Seismic reflections reveal a massive melt layer feeding Campi Flegrei caldera. *Geophys. Res. Lett.* **2008**, *35*, L12306. [CrossRef]

38.   Vanorio, T.; Virieux, J.; Capuano, P.; Russo, G. Three-dimensional seismic tomography from P wave and S wave microearthquake travel times and rock physics characterization of the Campi Flegrei Caldera. *J. Geophys. Res. Solid Earth* **2005**, *110*, B3. [CrossRef]

39.   Battaglia, J.; Zollo, A.; Virieux, J.; Iacono, D.D. Merging active and passive data sets in traveltime tomography: The case study of Campi Flegrei caldera (Southern Italy). *Geophys. Prospect.* **2008**, *56*, 555–573. [CrossRef]

40.   De Siena, L.; Amoruso, A.; Pezzo, E.D.; Wakeford, Z.; Castellano, M.; Crescentini, L. Space-weighted seismic attenuation mapping of the aseismic source of Campi Flegrei 1983–1984 unrest. *Geophys. Res. Lett.* **2017**, *44*, 1740–1748.

41.   De Siena, L.; Chiodini, G.; Vilardo, G.; Del Pezzo, E.; Castellano, M.; Colombelli, S.; Tisato, N.; Ventura, G. Source and dynamics of a volcanic caldera unrest: Campi Flegrei, 1983–84. *Sci. Rep.* **2017**, *7*, 1–13. [CrossRef]

42.   Calò, M.; Tramelli, A. Anatomy of the campi flegrei caldera using enhanced seismic tomography models. *Sci. Rep.* **2018**, *8*, 1–12. [CrossRef]

43. Siniscalchi, A.; Tripaldi, S.; Romano, G.; Chiodini, G.; Improta, L.; Petrillo, Z.; D'Auria, L.; Caliro, S.; Avino, R. Reservoir structure and hydraulic properties of the Campi Flegrei geothermal system inferred by audiomagnetotelluric, geochemical, and seismicity study. *J. Geophys. Res. Solid Earth* **2019**, *124*, 5336–5356. [CrossRef]

44. Troiano, A.; Di Giuseppe, M.G.; Patella, D.; Troise, C.; De Natale, G. Electromagnetic outline of the Solfatara–Pisciarelli hydrothermal system, Campi Flegrei (southern Italy). *J. Volcanol. Geotherm. Res.* **2014**, *277*, 9–21. [CrossRef]

45. Gresse, M.; Vandemeulebrouck, J.; Byrdina, S.; Chiodini, G.; Revil, A.; Johnson, T.C.; Ricci, T.; Vilardo, G.; Mangiacapra, A.; Lebourg, T.; et al. Three-dimensional electrical resistivity tomography of the Solfatara crater (Italy): Implication for the multiphase flow structure of the shallow hydrothermal system. *J. Geophys. Res. Solid Earth* **2017**, *122*, 8749–8768. [CrossRef]

46. Troise, C.; De Natale, G.; Schiavone, R.; Somma, R.; Moretti, R. The Campi Flegrei caldera unrest: Discriminating magma intrusions from hydrothermal effects and implications for possible evolution. *Earth Sci. Rev.* **2019**, *188*, 108–122. [CrossRef]

47. Moretti, R.; De Natale, G.; Troise, C. Hydrothermal versus magmatic: Geochemical views and clues into the unrest dilemma at Campi Flegrei. In *Vesuvius, Campi Flegrei, and Campanian Volcanism*; Elsevier: Amsterdam, The Netherlnads, 2020; pp. 371–406.

48. Chiodini, G.; Selva, J.; Del Pezzo, E.; Marsan, D.; De Siena, L.; D'auria, L.; Bianco, F.; Caliro, S.; De Martino, P.; Ricciolino, P.; et al. Clues on the origin of post-2000 earthquakes at Campi Flegrei caldera (Italy). *Sci. Rep.* **2017**, *7*, 1–10. [CrossRef]

49. Di Vito, M.A.; Isaia, R.; Orsi, G.; Southon, J.D.; De Vita, S.; d'Antonio, M.; Pappalardo, L.; Piochi, M. Volcanism and deformation since 12,000 years at the Campi Flegrei caldera (Italy). *J. Volcanol. Geotherm. Res.* **1999**, *91*, 221–246. [CrossRef]

50. De Martino, P.; Tammaro, U.; Obrizzo, F. GPS time series at Campi Flegrei caldera (2000–2013). *Ann. Geophys.* **2014**, *57*, S0213.

51. Petrillo, Z.; D'Auria, L.; Mangiacapra, A.; Chiodini, G.; Caliro, S.; Scippacercola, S. A perturbative approach for modeling short-term fluid-driven ground deformation episodes on volcanoes: A case study in the Campi Flegrei caldera (Italy). *J. Geophys. Res. Solid Earth* **2019**, *124*, 1036–1056. [CrossRef]

52. Istituto Nazionale di Geofisica e Vulcanologia. Osservatorio Vesuviano. Database Sismologico dei Vulcani della Campania. Available online: http://sismolab.ov.ingv.it/sismo/index.php?PAGE=SISMO/last&area=Flegrei&rmenu=on (accessed on 24 April 2020).

53. Chiodini, G.; Giudicepietro, F.; Vandemeulebrouck, J.; Aiuppa, A.; Caliro, S.; De Cesare, W.; Tamburello, G.; Avino, R.; Orazi, M.; D'Auria, L. Fumarolic tremor and geochemical signals during a volcanic unrest. *Geology* **2017**, *45*, 1131–1134. [CrossRef]

54. Aitchison, J. A new approach to null correlations of proportions. *Math. Geol.* **1981**, *13*, 175–189. [CrossRef]

55. Aitchison, J. The statistical analysis of compositional data (with discussion). *J. R. Stat. Soc.* **1982**, *B44*, 139–177.

56. Lowenstern, J.B. Carbon dioxide in magmas and implications for hydrothermal systems. *Miner. Deposita* **2001**, *36*, 490–502. [CrossRef]

57. Chiodini, G.; Marini, L. Hydrothermal gas equilibria: The H_2O-H_2-CO_2-CO-CH_4 system. *Geochim. Cosmochim. Acta* **1998**, *62*, 2673–2687. [CrossRef]

58. Reimann, C.; Filzmoser, P. Normal and lognormal data distribution in geochemistry: Death of a myth. Consequences for the statistical treatment of geochemical and environmental data. *Environ. Geol.* **2000**, *39*, 1001–1014. [CrossRef]

59. Shapiro, S.S.; Francia, R.S. An approximate analysis of variance test for normality. *J. Am. Stat.* **1972**, *67*, 215–216. [CrossRef]

60. Doornik, J.A.; Hansen, H. An omnibus test for univariate and multivariate normality. *Oxf. Bull. Econ. Stat.* **2008**, *70*, 927–939. [CrossRef]

61. Gordon, A.D. *Classification: Methods for the Exploratory Analysis of Multivariate Data*; Chapman and Hall: London, UK, 1981.

62. Ward, J.H., Jr. Hierarchical grouping to optimize an objective function. *J. Am. Stat. Assoc.* **1963**, *58*, 236–244. [CrossRef]

63. Spearman, C. The Proof and Measurement of Association between Two Things. *Am. J. Psychol.* **1904**, *15*, 72–101. [CrossRef]

64. Mann, H.B. Non-parametric tests against trend. *Econometrica* **1945**, *13*, 163–171. [CrossRef]

65. Kendall, M.G. *Rank Correlation Methods*, 4th ed.; Charles Griffin: London, UK, 1975.

66. Dickey, D.A.; Fuller, W.A. Distribution of the estimators for autoregressive time series with a unit root. *J. Am. Stat. Assoc.* **1979**, *74*, 427–431.

67. Akaike, H. Statistical predictor identification. *Ann. Inst. Stat. Math.* **1970**, *22*, 203–217. [CrossRef]

68. Hannan, E.J.; Quinn, B.G. The determination of the order of an autoregression. *J. R. Stat. Soc. Ser. B* **1979**, *41*, 190–195. [CrossRef]

69. Akaike, H. Information theory and an extension of the maximum likelihood principle. In Proceedings of the Second International Symposium on Information Theory, Tsahkadsor, Armenia, USSR, 2–8 September 1971; 1973; pp. 267–281.

70. Akaike, H. A new look at the statistical model identification. *IEEE Trans. Autom. Control* **1974**, *19*, 716–723. [CrossRef]

71. Hamilton, J.D.; Susmel, R. Autoregressive conditional heteroskedasticity and changes in regime. *J. Econ.* **1994**, *64*, 307–333. [CrossRef]

72. Dzurisin, D. A comprehensive approach to monitoring volcano deformation as a window on the eruption cycle. *Rev. Geophys.* **2003**, *41*, 1001. [CrossRef]

73. Voight, B.R.; Hoblitt, A.; Clarke, A.; Lockhart, A.; Miller, L.; Lynch, L.; McMahon, J. Remarkable cyclic ground deformation monitored in real-time on Montserrat, and its use in eruption forecasting. *Geophys. Res. Lett.* **1998**, *25*, 3405–3408. [CrossRef]

74. White, R.; McCausland, W. Volcano-tectonic earthquakes: A new tool for estimating intrusive volumes and forecasting eruptions. *J. Volcanol. Geotherm. Res.* **2016**, *309*, 139–155. [CrossRef]

75. Gottsmann, J.; Carniel, R.; Coppo, N.; Wooller, L.; Hautmann, S.; Rymer, H. Oscillations in hydrothermal systems as a source of periodic unrest at caldera volcanoes: Multiparameter insights from Nisyros, Greece. *Geophys. Res. Lett.* **2007**, *34*, L07307. [CrossRef]

76. Saccorotti, G.S.; Petrosino, F.; Bianco, M.; Castellano, D.; Galluzzo, M.; La Rocca, E.; Del Pezzo, L.; Zaccarelli, C.P. Seismicity associated with the 2004–2006 renewed ground uplift at Campi Flegrei Caldera, Italy. *Phys. Earth Planet. Inter.* **2007**, *165*, 14–24. [CrossRef]

77. D'Auria, L.; Giudicepietro, F.; Aquino, I.; Borriello, G.; Del Gaudio, C.; Lo Bascio, D.; Martini, M.; Ricciardi, G.P.; Ricciolino, P.; Ricco, C. Repeated fluid-transfer episodes as a mechanism for the recent dynamics of Campi Flegrei caldera (1989–2010). *J. Geophys. Res.* **2011**, *116*, B04313. [CrossRef]

78. Sibson, R.H.; Moore, J.M.M.; Rankin, A.H. Seismic pumping—A hydrothermal fluid transport mechanism. *J. Geol. Soc.* **1975**, *131*, 653–659. [CrossRef]

79. Todesco, M.; Rinaldi, A.P.; Bonafede, M. Modeling of unrest signals in heterogeneous hydrothermal systems. *J. Geophys. Res.* **2010**, *115*, B09213. [CrossRef]

80. Morrow, C.A.; Moore, D.E.; Lockner, D.A. Permeability reduction in granite under hydrothermal conditions. *J. Geophys. Res.* **2001**, *106*, 30551–30560. [CrossRef]

81. Heap, M.J.; Baud, P.; Meredith, P.G.; Vinciguerra, S.; Reuschlé, T. The permeability and elastic moduli of tuff from Campi Flegrei, Italy: Implications for ground deformation modelling. *Solid Earth* **2014**, *5*, 25. [CrossRef]

82. Stern, D.I.; Kaufmann, R.K. Anthropogenic and natural causes of climate change. *Clim. Change* **2014**, *122*, 257–269. [CrossRef]

83. Chiodini, G.; Caliro, S.; Avino, R.; Bagnato, E.; Capecchiacci, F.; Carandente, A.; Cardellini, C.; Minopoli, C.; Tamburello, G.; Tripaldi, S.; et al. Forthcoming. The Campi Flegrei hydrothermal system. In *Campi Flegrei*; Orsi, G., Civetta, L., D'Antonio, M., Eds.; ISBN 978-3-642-37060 in Book Series "Active Volcanoes of the World"; Springer Verlag: Berlin, Germany.

84. Ricco, C.; Petrosino, S.; Aquino, I.; Del Gaudio, C.; Falanga, M. Some investigations on a possible relationship between ground deformation and seismic activity at Campi Flegrei and Ischia volcanic areas (Southern Italy). *Geoscience* **2019**, *9*, 222. [CrossRef]

85. Cappa, F.; Rutqvist, J.; Yamamoto, K. Modeling crustal deformation and rupture processes related to upwelling of deep CO_2-rich fluids during the 1965–1967 Matsushiro earthquake swarm in Japan. *J. Geophys. Res.* **2009**, *114*, B10304. [CrossRef]

86. Yukutake, Y.; Honda, R.; Harada, M.; Arai, R.; Matsubara, M. A magma-hydrothermal system beneath Hakone volcano, central Japan, revealed by highly resolved velocity structures. *J. Geophys. Res. Solid Earth* **2015**, *120*, 3293–3308. [CrossRef]

87. Ohba, T.; Yaguchi, M.; Nishino, K.; Numanami, N.; Daita, Y.; Sukigara, C.; Masanori, I.; Tsunogai, U. Time variations in the chemical and isotopic composition of fumarolic gases at Hakone volcano, Honshu Island, Japan, over the earthquake swarm and eruption in 2015, interpreted by magma sealing model. *Earth Planets Space* **2019**, *71*, 48. [CrossRef]

88. Geweke, J. Measurement of linear dependence and feedback between multiple time series. *J. Am. Stat.* **1982**, *77*, 304–313. [CrossRef]